A. C. Bernal Ayala, J. J. Gerth, T. J. Schmit, S. S. Lindstrom, and J. P. Nelson III, 2023: Parallax shift in *GOES* ABI data. *J. Operational Meteor.,* **11** (2), 14-23, doi: https://doi.org/10.15191/nwajom.2023.1102.

Journal of Operational Meteorology
Short Contribution

Parallax Shift in *GOES* ABI Data

ANTHONY C. BERNAL AYALA
Department of Atmospheric and Oceanic Sciences, University of Wisconsin-Madison, Madison, Wisconsin
National Weather Service Office of Observations, Silver Spring, Maryland

JORDAN J. GERTH
National Weather Service Office of Observations, Silver Spring, Maryland

TIMOTHY J. SCHMIT
NOAA/NESDIS Center for Satellite Applications and Research, Advanced Satellite Products Branch, Madison, Wisconsin

SCOTT S. LINDSTROM
Cooperative Institute for Meteorological Satellite Studies (CIMSS), University of Wisconsin-Madison, Madison, Wisconsin

JAMES P. NELSON III
Cooperative Institute for Meteorological Satellite Studies (CIMSS), University of Wisconsin-Madison, Madison, Wisconsin

(Manuscript received 14 June 2022; review completed 12 December 2022)

ABSTRACT

A parallax shift is a displacement in the apparent navigated position of a feature that arises because of its perspective from the viewing platform and is also a function of the feature height. For Geostationary Operational Environmental Satellite (*GOES*) imagery, this shift is especially apparent away from the satellite subpoint. Users should understand the degree of this shift when combining *GOES* Advanced Baseline Imager (ABI) imagery with other data, such as radar and lightning. However, it can be challenging, especially at spatial resolutions around the cloud/storm scale. This article explores parallax displacement for both uniform and computed cloud-top heights. Parallax shift will be shown using two case studies. The first case is from 7 September 2021, in which northern Illinois hailstorms are examined using ground-based Level II NEXRAD radar data, *GOES-16* ABI imagery, and Geostationary Lightning Mapper data. The second case, on 9 April 2021, examines an eruption of the La Soufrière volcano on St. Vincent from the differing perspectives of *GOES-16* and *-17*. The discussion of these cases will show how parallax is an apparent displacement that will vary depending on what satellites are used for observation, where the phenomenon is with respect to the satellite, and the height of the phenomenon being analyzed. Newer satellite instruments with finer spatial resolutions and improved georeferencing will maximize data usability at more extreme angles and require users to account for the accompanying enhanced parallax shift. Even at lesser angles, parallax displacement is an important consideration for many meteorological and other applications.

1. Introduction

In satellite meteorology, parallax displacement is a shift in the apparent (or mapped) position along a reference ellipsoid of Earth's surface or atmospheric features (e.g., high terrain, clouds, lightning) due to non-nadir viewing geometry (AMS 2019). In geostationary satellite data, this shift is especially apparent when well-developed convective features are compared to ground-based radar data with little significant parallax shift, displacing a storm a significant distance away from its radar presentation. With the *Geostationary Operational Environmental Satellite* (*GOES-R*) series Advanced Baseline Imager (ABI) data (Schmit et al. 2018), more observations of different channels that exhibit parallax shifts are seen by operational meteorologists, as well as by a wide range of users (e.g., graduate students, recreational weather enthusiasts) who may not be considering this shift when interpreting and analyzing *GOES* datasets.

Corresponding author address: Anthony C. Bernal Ayala, 1225 West Dayton Street, Madison, WI 53706
E-mail: crespo3@wisc.edu

Furthermore, the greater spatial resolution of ABI data leads to more uses of satellite imagery on finer scales where the effects of parallax are more noticeable. The overall goal of this paper is to bring increased awareness of parallax to a broad user base of *GOES* ABI data by explaining the shift, showing examples of why it must be considered, and providing a means to correct it.

The ABI scans the Earth with a number of detectors, and then a group of detectors is used to build a pixel value projected on a fixed grid (Kalluri et al. 2018). The mathematical solution requires intimate knowledge of the satellite orbit, including the satellite view angle, and it is performed under the assumption of clear skies. Infrared radiation sensed by the satellite instrument is emitted (or, in the case of visible or near-infrared radiation, reflected) from the earth's surface or near-surface features and travels to the satellite. C. Wang and X. Huang (2014) describe a general solution to the parallax correction issue concerning the collocation of measurements of the same object from different satellites that use different viewing geometries. Their paper highlights the importance of accurate collocation to avoid introducing incorrect information in the data fusion of multiple sensors on different satellite platforms. Parallax can be represented as a displacement vector $|\vec{r}|$ as shown in Fig. 1 and can be defined as follows:

$$|\vec{r}| = \frac{hH\tan\theta}{(H-h)} \sim h\tan\theta \quad (1)$$

where H is the altitude of the satellite [36 000 km (22 369 mi) for the geostationary orbit], h is the cloud-top height, and θ is the viewing zenith angle of the sensor at the cloud base. If the sensor-viewing azimuth angle is denoted as φ and the latitude and longitude of the cloud base as Y_D and X_D in radians, respectively, the displacement vector can be projected onto latitude and longitude, and thus the non-parallax-corrected coordinates can be determined via:

$$\begin{aligned} Y_E &= Y_D + \frac{|\vec{r}|\cos\cos\emptyset}{R_E} \\ X_E &= X_D + \frac{|\vec{r}|\sin\sin\emptyset}{(R_E\cos\cos Y_D)} \end{aligned} \quad (2)$$

where all angles and coordinates are in radians, and RE is the radius of the Earth [~6371 km (3959 mi)]. Additionally, the distance between two points along a great circle of a sphere can be expressed as:

$$\widehat{AB} = \arccos(\sin Y_A \sin Y_B + \cos Y_A \cos Y_B \cos(X_A - X_B)) \quad (3)$$

Clouds and other objects (e.g., wildfire smoke) can block the satellite view of the Earth's surface (Fig. 2). Energy that reaches the satellite sensor will be mapped to the earth's surface, even if the energy's origin is from the top or side of a cloud that has developed along the line-of-sight view of the surface location. This is the origin of the parallax shift. When georeferencing the cloud feature, satellite navigation assumes that the feature is located at the earth's surface along a straight line from the satellite to where the line intersects the cloud. The cloud pixel will then be georeferenced at this perceived location some distance poleward from its true earth location. The shift of the satellite-detected feature to its true earth location is always toward the satellite subpoint. In other words, a non-parallax-corrected cloud is presented at a location that is too far away from the satellite subpoint (as displayed by location D in Fig. 1). Parallax shift magnitude is a function of the satellite zenith angle, the latitude difference between the satellite subpoint and the true earth location of the feature, and cloud height. Taller clouds and clouds farther away from the satellite subpoint likewise have a larger parallax shift. The next section quantifies this

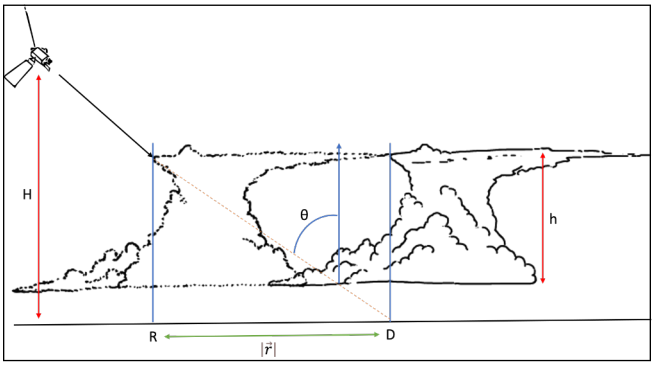

Figure 1. Schematic showing the viewing geometries of a satellite to illustrate parallax shift. Note that this drawing is for illustration only; hence, horizontal and vertical dimensions are not to scale. Point R represents the real geolocation of the cloud pixel, point D represents the displaced location of the cloud pixel. This figure is reproduced from a United States government presentation based on the work of Chad Gravelle. *Click image for an external version; this applies to all figures hereafter.*

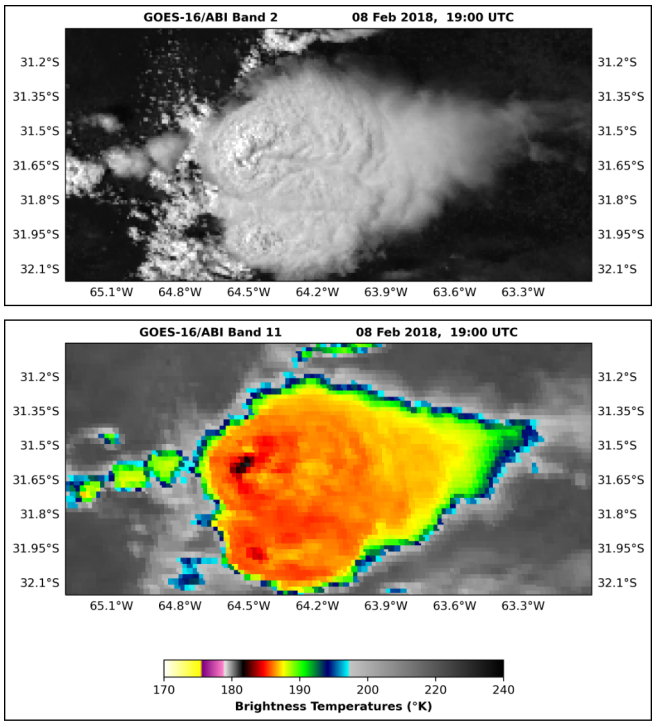

Figure 2. Satellite navigation example for a tall cloud from *GOES-16* ABI bands 2 (a) and 11 (b) with approximate wavelengths of 0.64 and 8.4 μm, respectively. Although some radiance information originates from the side of the cloud, the navigation algorithm places that information at a point farther from the satellite subpoint.

parallax shift in the context of cloud-top height and as a function of latitude. Section 3 highlights the importance of parallax awareness when fusing *GOES* ABI data with other common remote-sensing and surface-based datasets. The remainder of the paper summarizes the operational implications of geostationary satellite imagery parallax shift, with an appendix offering a method to correct for parallax in *GOES* ABI data.

2. The amount of apparent shift

Parallax shift can be computed for a particular cloud height, and the magnitude of the shift is manifested as concentric circles around the satellite subpoint. For example, the *GOES-16* (*GOES-East*) and *GOES-17* (*GOES-West*) parallax shift for a uniform 3.05-km (10 000-ft) cloud deck is shown in Fig. 3. Depending on which satellite is taking the measurement, the parallax shift over the contiguous United States will point toward the southeast and then

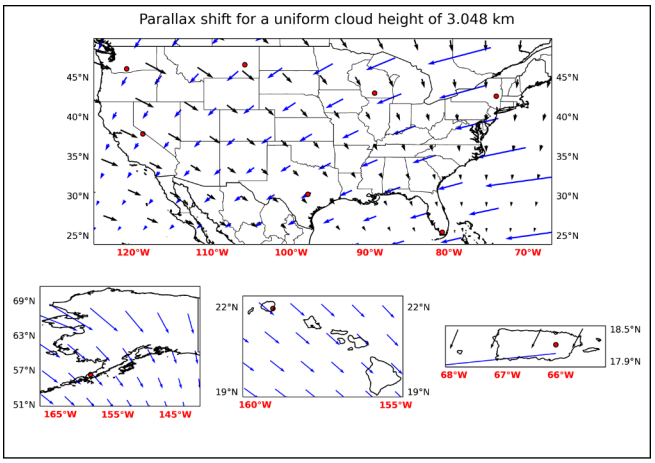

Figure 3. Computed parallax shift from the *GOES-East* and *GOES-West* satellite positions for a uniform cloud height of 3.05 km (10 000 ft) over the contiguous United States (a), Alaska (b), Hawaiian Islands (c), and Puerto Rico (d). Black arrows show the parallax shift away from the *GOES-East* satellite subpoint (nominally 0ºN, 75ºW), blue arrows show the parallax shift away from the *GOES-West* satellite subpoint (nominally 0ºN, 137ºW). Arrows were lengthened 10 times.

south as a cloud feature gets closer to the *GOES-16* satellite subpoint at approximately 0ºN, 75ºW, and point towards the southwest and then south as a cloud feature gets closer to the *GOES-17* satellite subpoint at approximately 0ºN, 137ºW. As seen in Table 1, the apparent shift ranges over the contiguous United States from 1.81 km (1.1 mi)—that is, about 1 *GOES-16* infrared pixel—over Florida to greater than 8 km (5 mi, about 5 infrared pixels) over Washington and the Pacific Northwest. The parallax shift increases for taller clouds except near the satellite subpoint, where parallax effects are minimal. For a uniform 15.25-km (50 000-ft) cloud deck, as seen in Table 1 and plotted in Fig. 4, the parallax shift ranges from 9 km (5.6 mi) over Florida to more than 40 km (25 mi) over Washington and the Pacific Northwest. Fortunately, specific cloud-top height information can be provided by algorithms such as the Algorithm Working Group (AWG) Cloud Height Algorithm (ACHA) (Heidinger and Li 2017), which uses spectral information provided by the *GOES-R* ABI to derive cloud-top heights. This data can then be used to correct parallax shifts, as shown in Table 2 and Fig. 5 for 13 April 2022 at 1420 UTC.

Table 1. Computed parallax shift for specific locations across the United States (represented by red dots in Figs. 3, 4, 5) from the *GOES-East* and *GOES-West* satellites, assuming uniform cloud heights of 3.05 km (10 007 ft) and 15.24 km (50 000 ft).

		GOES-16		*GOES-17*	
Location	**Coordinates**	**3-km adjustment (km)**	**15-km adjustment (km)**	**3-km adjustment (km)**	**15-km adjustment (km)**
Mount Adams, WA	46.17°N, 120.85°W	8.15	40.41	4.46	22.22
Madison, WI	43.10°N, 89.43°W	3.91	19.51	7.87	39.05
Altamont, NY	42.72°N, 74.03°W	3.58	17.84	- - - -	- - - -
Twin Buttes, MT	46.70°N, 105.89°W	5.70	28.35	5.72	28.47
Austin, TX	30.32°N, 97.90°W	2.88	14.37	4.41	21.98
Eastern Sierra, CA	37.97°N, 118.80°W	6.04	30.05	3.39	16.89
Everglades, FL	25.55°N, 80.86°W	1.81	9.01	7.57	37.58
Lake and Peninsula, AK	56.37°N, 159.75°W	- - - -	- - - -	7.40	36.75
Kauai, HI	21.98°N, 159.37°W	- - - -	- - - -	2.23	11.12
Caguas, PR	18.23°N, 66.09°W	1.34	6.68	- - - -	- - - -

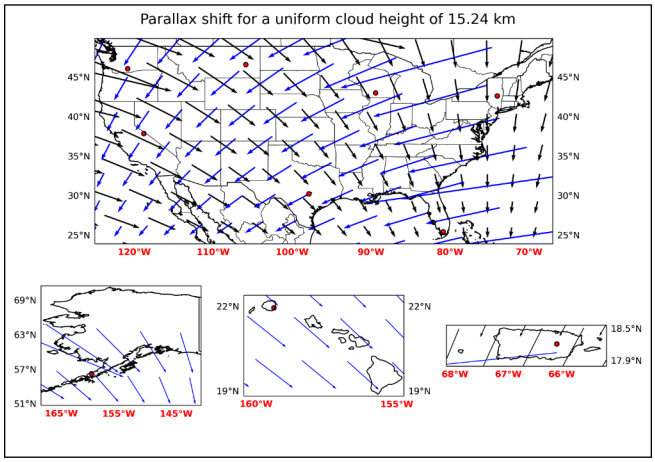

Figure 4. Computed parallax shift from the *GOES-East* and *GOES-West* satellite positions for a uniform cloud height of 15.24 km (50 000 ft) United States (a), Alaska (b), Hawaiian Islands (c), and Puerto Rico (d). Black arrows show the parallax shift away from the *GOES-East* satellite subpoint (nominally 0ºN, 75ºW), blue arrows show the parallax shift away from the *GOES-West* satellite subpoint (nominally 0ºN, 137ºW). Arrows were lengthened 10 times.

3. Fusing satellite imagery with other data

a. 7 September 2021, Illinois hailstorm

What are the operational implications of geostationary satellite imagery parallax shift? It is important to consider the shift when comparing geostationary satellite imagery to geospatial data from other sources with little to no parallax shift or perhaps having a parallax shift that has been corrected assuming a constant feature height. For example, Geostationary Lightning Mapper (GLM) Level 1B data (Virts and Koshak 2020) corrects the parallax shift with a constant cloud height of 12.5 km (41 011 ft). In Fig. 6, Level II NEXRAD radar data show numerous bands of severe thunderstorms moving through northern Illinois and parts of northwest Indiana on 7 September 2021. The thunderstorms were supercells characterized by their rotating updrafts.

Significant hail larger than golf balls fell in parts of Lee and LaSalle Counties, including near and in the towns of West Brooklyn, Compton, Paw Paw, and Earlville, with some of the hail not melting until several hours after it fell (NWS 2021). When looking at 1.5-degree Level II NEXRAD radar images at 1901 UTC from KLOT (Lewis University Airport in Chicago/Romeoville, Illinois), a continuous area of high reflectivity is identified over Compton, Sublette, and Paw Paw, Illinois, associated with a hail report at 1901 UTC at Compton, Illinois. A secondary continuous area of high reflectivity is identified extending from East Forest, Highland Park, Lincoln Shore, and nearby cities. When overlayed with data from the *GOES-16* ABI imagery 8.4 μm band, an area of low-brightness temperature (operational meteorologists often refer to this feature as "cold cloud tops") along the western convective core is observed northwest of the area of high radar reflectivity over Compton and nearby cities and is located at approximately 41.63ºN, 89.25ºW. A second, northern convective core of low-brightness temperatures in satellite imagery is identified northwest

Table 2. Computed parallax shift for specific locations across the United States from the *GOES-East* and *GOES-West* satellites for various cloud heights determined via the *GOES* ACHA cloud-top height algorithm for 13 April 2022 at 14:20 UTC.

	GOES-16		***GOES-17***	
Location	**Cloud-top height (km)**	**Adjustment for parallax using cloud-top height (km)**	**Cloud-top height (km)**	**Adjustment for parallax using cloud-top height (km)**
Mount Adams, WA	No cloud	No cloud	No cloud	No cloud
Madison, WI	9.63	12.35	No cloud	No cloud
Altamont, NY	2.99	2.28	- - - -	- - - -
Twin Buttes, MT	2.64	12.19	No cloud	No cloud
Austin, TX	1.84	1.87	No cloud	No cloud
Eastern Sierra, CA	6.08	8.25	6.12	4.00
Everglades, FL	12.48	6.72	2.13	6.64
Lake and Peninsula, AK	- - - -	- - - -	No cloud	No cloud
Kauai, HI	- - - -	- - - -	5.91	4.32
Caguas, PR	1.84	0.81	- - - -	- - - -

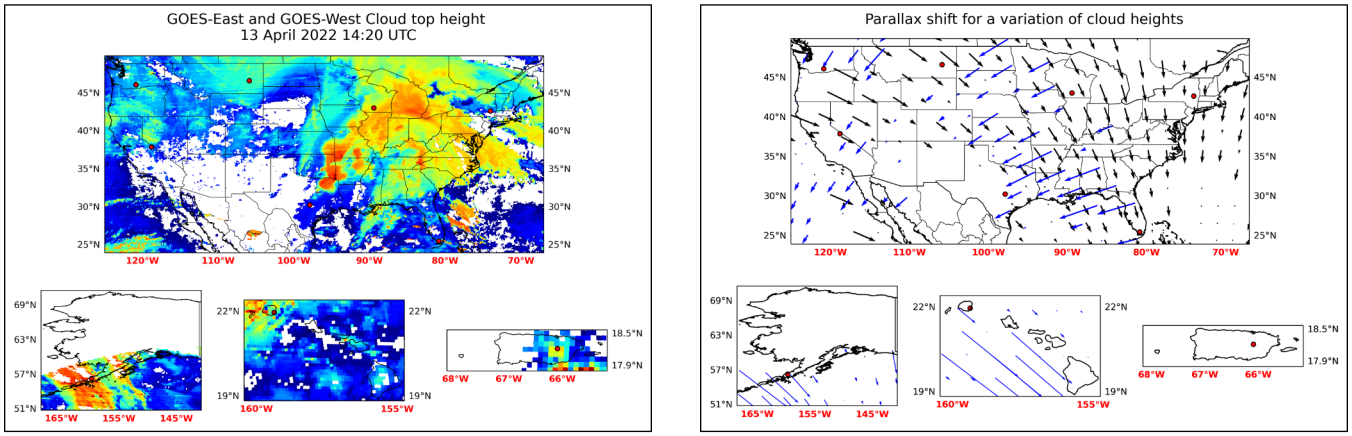

Figure 5. (a) *GOES* ACHA cloud-top height product used to compute (b) the parallax shift from the *GOES-East* and *GOES-West* satellite positions for various cloud heights and regions. Black arrows show the parallax shift away from the *GOES-East* satellite subpoint (nominally 0ºN, 75ºW), blue arrows show the parallax shift away from the *GOES-West* satellite subpoint (nominally 0ºN, 137ºW). Arrows were lengthened 1.75 times.

of Lake Forest and nearby cities at approximately 42.38ºN, 88ºW.

When using the computed *GOES-16* cloud-top heights for these convective clouds, the western convective core has a cloud-top height of 11.5 km (approximately 37 730 ft), yielding a 14.14 km (8.79 mi) parallax shift. The northern convective core has a cloud-top height of 14.1 km (approximately 46 260 ft), yielding a 13.92 km (8.65 mi) parallax shift. The parallax shifts for both convective cores are south-southeast of the initially calculated latitude and longitude coordinates. When GLM (specifically flash extent density "FED" data) is superimposed over the radar imagery (Fig. 6, bottom figure), other apparent shifts are evident between areas of high reflectivity and high flash density. When looking at the area of continuous high reflectivity that was previously correlated with the western convective core over Lee and DeKalb counties, a flash density echo extends through the area of high reflectivity. Still, the region with the highest flash density is north of the continuous area of high reflectivity. Similarly seen in ABI imagery, flash density data over the eastern continuous area of high reflectivity associated with the eastern convective cell over Lake County and Lake Michigan appear shifted northwest of the area of continuous high reflectivity. This example shows why satellite data users must be aware of parallax shifts to properly interpret satellite information.

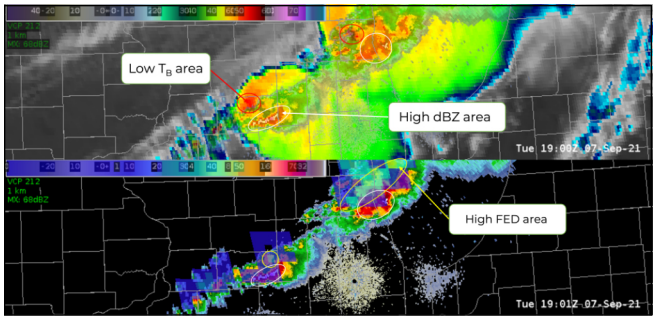

Figure 6. Panel (a) Shows *GOES-16* ABI "Cloud Top Phase Band" (8.4 μm) color-enhanced brightness temperature (TB) at 1900 UTC with shaded Level II NEXRAD radar data at 1.5º scan angle for 1901 UTC 07 September 2021. Panel (b) Shows Level II NEXRAD radar data at a 1.5º scan angle for 1901 UTC with shaded GLM 1-min flash density data on the same date. Reference imagery from AWIPS.

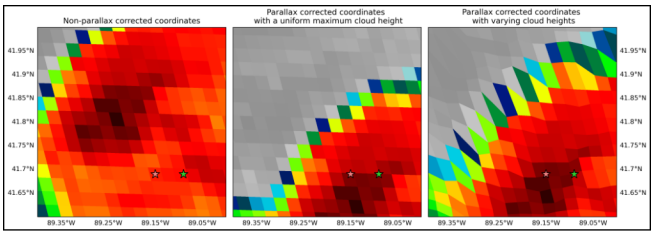

Figure 7. *GOES-16* ABI "Cloud Top Phase Band" (8.4 μm) color-enhanced brightness temperature at 1900 UTC 7 September 2021 shows one convective core (area of low-brightness temperatures) compared to surface hail reports represented by stars (light-coral star is associated with a report at 1859 UTC and lime-green star is associated with a report at 1901 UTC). Note the distance between the convective core and the surface hail reports before parallax correction (a) and after parallax correction using the maximum cloud height (b) and varying cloud heights (c).

Figure 7 shows *GOES-16* ABI data plotted against non-parallax-corrected coordinates, parallax-corrected coordinates with uniform maximum cloud height, and parallax-corrected coordinates with varying cloud heights using the ACHA data file. Additionally, two hail reports are used as reference points when correcting parallax: the first report at 1859 UTC (a light coral-colored star) and the second hail report at 1901 UTC (represented by the lime-green-colored star). This figure shows the importance of considering parallax when analyzing any ABI product with a combination of surface-based observations. The figure on the left shows a considerable distance (approximately 22.4 km or 13.92 mi) between the hail reports and the area of low-brightness temperatures. When the shift is corrected with the maximum cloud height [Fig. 7, middle figure, in this case, the cloud-top height was 18.04 km (59 186 ft)], there is a more accurate estimation of where the area of low-brightness temperature was located at the measurement time.

On the other hand, when using a variety of cloud-top heights to correct each individual pixel (rightmost figure), the low-brightness temperature shows a small displacement, still important to highlight when correlated with hail reports. This small displacement compared to the location when the maximum cloud-top height was used can come from an overestimation of the cloud height leading to a less accurate location of that low-brightness temperature pixel. This comparison between using the maximum cloud-top height versus varying cloud-top heights is important to show because it proves what has been discussed in previous sections and gives the reader a reference on how impactful parallax shift can be in analyzing satellite data when they are correlated to other surface-based data. Refer to the appendix for further explanation on parallax correction.

b. 9 April 2021, La Soufrière volcanic eruption

This case study will examine the parallax shift between *GOES-16* and *-17* within ABI imagery products. On 9 April 2021, the La Soufrière volcano on St. Vincent Island (approximately 13ºN, 61ºW) erupted for the first time in 40 years, sending an ash plume 10 km (6 mi) into the sky (IFRC 2021). Multiple subsequent eruptions also occurred, and several tropical storms and rain events hampered cleanup operations and slowed the recovery phase. Although heavy ashfall initially impacted the surrounding islands, Barbados, Grenada, and St. Lucia avoided suffering significant damage or evacuation notices. Figure 8, shows *GOES-16* (top figure) and *-17* (bottom figure) true color red-green-blue (RGB) composite imagery (Bah et al. 2018) coverage of the volcanic eruption at 1930 UTC. It is evident from the figures that the parallax displacement associated with the large viewing angle from *GOES-17* [the shift ranges from 32.08 km (20.38 mi) for a 3.05 km (10 007 ft) cloud-top height to 146.00 km (91 mi) for a 15.24 km (50 000 ft) cloud-top height toward the west-southwest; Fig. 8, bottom figure] is much larger than the parallax shift from *GOES-16* [the shift ranges

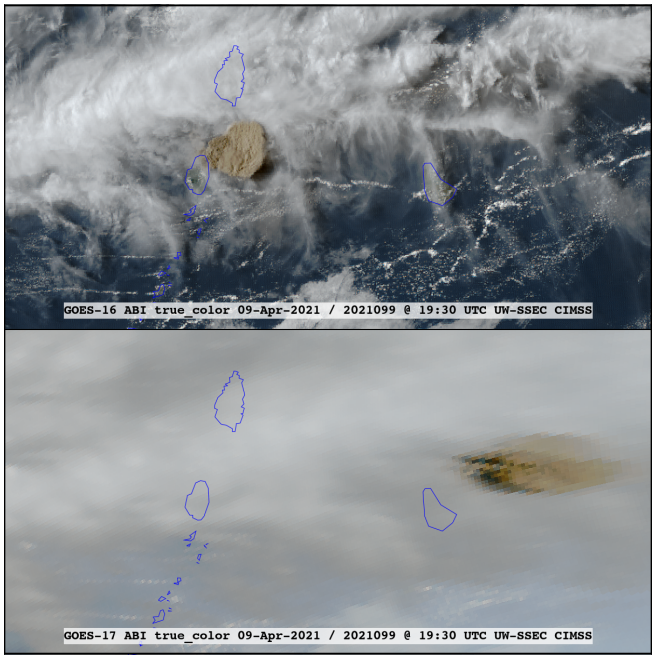

Figure 8. True color RGB imagery from (a) *GOES-16* and (b) *GOES-17* at 1930 UTC 9 April 2021 showing the ash cloud from the La Soufrière volcanic eruption. Note the large difference in parallax displacement from each satellite's perspectives.

from 1.26 km (0.78 mi) for a 3.05 km (10 007 ft) cloud-top height to 6.28 km (3.9 mi) for a 15.24 km (50 000 ft) cloud-top height toward the southwest; Fig. 8, top figure].

4. Operational applicability

In assessing atmospheric phenomena, operational meteorologists must regularly reconcile different datasets with unique perspectives in making forecast and warning decisions. For warning decisions, high-temporal resolution is a benefit for monitoring storm evolution and a compounding factor for operations. Meteorologists who participate in the NOAA Hazardous Weather Testbed Experimental Warning Program have long noted the challenges of mentally combining and building their conceptual model in real time with three commonly used observational platforms that provide geospatial data that contribute to the warning decision: radar, which is usually rendered as a plan-view slice through a storm at a given elevation; satellite, which shows the top or side of the storm, as discussed in this paper; and terrestrial lightning networks, which provide singular points representing the centroid of lightning flashes and strikes. None of these provide precise ground conditions, which is the ultimate basis for warnings to the public.

Although more sophisticated imagery approaches that involve correcting individual pixels based on their perceived height above ground have some promise (e.g., Rabin 2014), the long-term goal for the work described in this paper is to provide meteorologists with arrows to help match the storm presentation on satellite to its appearance on the radar without distortion. For example, a large convective cell and anvil can obscure developing convective towers depending on the direction of the satellite. The arrow technique is thus anticipated to be particularly helpful for multi-cell storm environments with storms at different stages of maturity and observed with significant satellite zenith angles. However, not all scenarios require such techniques. For mature supercells at lesser satellite zenith angles, developing the conceptual model (including the identification of the inflow region, anvil expansion, and storm-top outflow) is straightforward (e.g., EWP Blog 2015).

5. Conclusions

High-altitude cloud features (such as thunderstorm cloud tops) observed by either geostationary or low-earth orbit satellite sensors will appear to be displaced (to the north, south, east, or west) from other (relatively) near-surface datasets. The displacement is not an error. It is due to a phenomenon known as parallax, a displacement in the apparent navigated position of a feature that arises because of its perspective from the viewing platform. This shift can be significant when clouds are tall, far from the satellite subpoint, or both. A discussion of two cases shows how parallax is an apparent displacement that varies depending on which satellite(s) is used to observe a feature, where the feature is located with respect to the satellite, and the feature's height.

The development and application of algorithms that correct for parallax are essential for any user intending to use satellite products for a case study and operational weather forecasting purposes. This is especially true for regions of the world where there is not an extensive network of ground-based radar data available to study a specific phenomenon in detail. Owing to time constraints, efficiency is paramount in any parallax-correction algorithm involving imagery needed for short-term weather forecasting. Previously, parallax-corrected *GOES-14* (105ºW) 1-min imagery was tested

by National Weather Service (NWS) forecasters in the 2016 NOAA Hazardous Weather Testbed in Norman, OK, which placed thunderstorm tops near the core of lightning activity. Unfortunately, the correction process also introduced image artifacts in regions of the imagery without observations because of cloud blocking.

Other examples showing parallax have been documented in several University of Wisconsin-Madison CIMSS Satellite Blog posts (cimss.ssec.wisc.edu/satellite-blog/?s=parallax). These include *GOES* and low earth orbit sensors and applications ranging from fires to convection to volcanic ash clouds. With advances in the next generation of ABI products, newer satellite instruments with finer spatial resolutions and improved georeferencing will maximize data usability at more extreme angles and require users to account for the enhanced parallax shift. Even at smaller angles, parallax displacement is an important consideration for many meteorological or other applications. It is important to remember that parallax shift is a displacement of satellite imagery that does exist and needs to be accounted for when using satellite imagery operationally, academically, or when combining observational data involving different perspectives/platforms.

To further demonstrate the concept of parallax, users can go to the website (Whittaker 2014) developed at the University of Wisconsin-Madison, which shows many different sectors that can be accessed for reference when considering parallax shifts. The website includes imagery from the Himawari-8, *GOES-West*, and *GOES-East* satellites and parallax information covering the full disk, contiguous United States, Alaska, and much of Canada.

Acknowledgments. The views, opinions, and findings of this report are those of the authors. They should not be construed as an official National Oceanic and Atmospheric Administration or United States government position, policy, or decision. ABI data are archived at NOAA's CLASS: www.class.noaa.gov/. Other *GOES-16* cases can be found at the CIMSS Satellite Blog: cimss.ssec.wisc.edu/goes/blog/archives/category/goes-16. This research was partly supported by a NOAA grant to the Cooperative Institute for Meteorological Satellite Studies at the University of Wisconsin-Madison (NA15NES4320001). Thanks to Chad Gravelle and his team (NWS Training Center 2017) for providing all elements used to create Fig. 1. The authors want to acknowledge the NOAA/CIMSS Cloud Group, which provided the *GOES-16* ACHA data netCDF. Geo2grid software (cimss.ssec.wisc.edu/csppgeo/geo2grid.html) was used to generate Figure 8. We would also like to thank the anonymous reviewers and Dr. Angela K. Rowe for the quick and thorough comments that improved this paper. This work was supported as part of an internship with the National Weather Service, Office of Observations.

APPENDIX A

Method for Correcting for Parallax in *GOES* ABI Data

To make a parallax shift adjustment to any *GOES* ABI product, the user needs first to acquire the *GOES* ABI product file for the specific date and time of interest. In this case, 7 September 2021 at 1900 UTC was used. Additionally, the Level 1B radiances data file of Band 11 (8.4 μm) was the product picked to adjust the parallax shift, and the Level 2 ACHA data file was used as the cloud-top heights source for parallax correction. After accessing both files, methods presented in Hrisko (2018) were used to calculate latitude and longitudes from the *GOES-R* coordinate grid. Once latitude and longitude coordinates were extracted and calculated, brightness temperatures were converted from the radiances, following procedures explained in Schmit et al. (2012). After obtaining latitudes, longitudes, and brightness temperatures, latitude and longitude parallax shifts were computed using the theory discussed in C. Wang and X. Huang (2014) and Bieliński (2020), allowing for accurate latitude and longitude when adjusting the GOES ABI data. Users should remember that the ACHA data file available when this paper was written has a different spatial resolution than the Level 1B radiance data file. Because both data files need to be at the same spatial resolution to correct the parallax shift accurately, users will need to either downsize the pixel size in the Level 1B radiance data file or request the full-resolution ACHA data file directly from the appropriate authority. In this case, the full-resolution ACHA data file was available, which made this comparison possible. After both files are at the same resolution, the user has two options to correct the shift. The user can use the maximum cloud height from the ACHA data file and apply this height uniformly to all the pixels in the image or use the masked array of varying cloud heights and correct each brightness temperature pixel individually, resulting in the parallax-corrected latitude and longitude (as shown in Fig. 7).

REFERENCES

American Meteorological Society (AMS), 2019: Glossary of Meteorology: Parallax. [Available online at glossary.ametsoc.org/wiki/Parallax.]

Bah, M. K., M. M. Gunshor, and T. J. Schmit, 2018: Generation of *GOES-16* true color imagery without a green band. *Earth Space Sci*., **5**, 549–558, CrossRef.

Bieliński, T., 2020: A parallax shift effect correction based on cloud height for geostationary satellites and radar observations. *Remote Sens*., **12**, 365, CrossRef.

EWP Blog, 2015: Combining SRSO and radar data. [Available online at inside.nssl.noaa.gov/ewp/2015/06/11/combining-srso-and-radar-data/.]

Heidinger, A., and Li, Y., 2017: AWG cloud height algorithm (ACHA). NOAA NESDIS STAR Center for Satellite Applications and Research [Available online at www.star.nesdis.noaa.gov/goesr/documents/ATBDs/Enterprise/ATBD_Enterprise_Cloud_Height_v3.1_Mar2017.pdf.]

Hrisko, J., 2018: *GOES-R* satellite latitude and longitude grid projection algorithm. [Available online at makersportal.com/blog/2018/11/25/goes-r-satellite-latitude-and-longitude-grid-projection-algorithm.]

International Federation of Red Cross and Red Crescent Societies (IFRC), 2021: *Saint Vincent and the Grenadines and surrounding countries: La Soufrière volcanic eruption*, Emergency Appeal n° MDRVC005: 6-month operation update. [Available online at reliefweb.int/sites/reliefweb.int/files/resources/MDRVC005ou3.pdf.]

Kalluri, S., and Coauthors, 2018: From photons to pixels: Processing data from the Advanced Baseline Imager. *Remote Sens*., **10**, 177, CrossRef.

NWS, 2021: September 7, 2021: Swaths of large hail and damaging winds across northern Illinois. [Available online at www.weather.gov/lot/2021sept07.]

NWS Training Center2017: Satellite parallax: Causes and effects. [Available online at www.youtube.com/watch?v=MJQYCNPiNzA.]

Rabin, R., 2014: *GOES* visible and infrared imagery: Oklahoma and southern Plains. [Available online at www.ssec.wisc.edu/~rabin/ok.]

Schmit, T., M. Gunshor, G. Fu, T. Rink, K. Bah, W. Zhang, and W. Wolf, 2012: *GOES-R Advanced Baseline Imager (ABI) algorithm theoretical basis document for Cloud and Moisture Imagery Product (CMIP)*. NOAA NESDIS STAR Center for Satellite Applications and Research. [Available online at www.star.nesdis.noaa.gov/goesr/docs/ATBD/Imagery.pdf.]

Schmit, T. J., S. S. Lindstrom, J. J. Gerth, and M. M. Gunshor, 2018: Applications of the 16 spectral bands on the Advanced Baseline Imager (ABI). *J. Operational. Meteor*., **6**, 33–46, CrossRef.

Virts, K. S., and W. J. Koshak, 2020: Mitigation of geostationary lightning mapper geolocation errors. *J. Atmos. Ocean. Technol*., **37**, 1725–1736, CrossRef.

Wang, C. and X. Huang, 2014: Parallax correction in the analysis of multiple satellite data sets. *IEEE Geoscience and Remote Sensing Letters*, **11**, 965–969, CrossRef.

Whittaker, T., 2014: Parallax from geostationary satellites. [Available online at cimss.ssec.wisc.edu/goes/webapps/parallax/overview.html.]